

Article

Performance Comparison of Mini-Rectangular Fin Heat Sinks Using Different Coolants: Supercritical CO₂, Water and Al₂O₃/H₂O Nanofluid

Asem Alemam ¹, Sherif A. Yehya ¹, Abubaker S. Omer ¹, Ameer Hamza ¹, Muhammed Saeed ^{1,2}
and Abdallah S. Berrouk ^{1,3,*}

¹ Mechanical Engineering Department, Khalifa University of Science and Technology, Abu Dhabi P.O. Box 127788, United Arab Emirates

² Abu Dhabi Maritime Academy, Abu Dhabi P.O. Box 54477, United Arab Emirates

³ Center for Catalysis and Separation (CeCas), Khalifa University of Science and Technology, Abu Dhabi P.O. Box 127788, United Arab Emirates

* Correspondence: abdallah.berrouk@ku.ac.ae

Abstract: Mini-channel heatsinks have proven useful in removing high heat fluxes from microelectronic devices. However, further miniaturization of electronic devices requires significant enhancement in the mini-channel heatsinks' thermohydraulic characteristics, which depend greatly on the coolant and geometrical configuration of the channel. Therefore, the current study explores the potential of mini-channel heatsinks' using different coolants (water, nanofluid and supercritical carbon dioxide) and various channel configurations. The effect of various channel configurations on the thermohydraulic characteristics of the mini-channel heat sinks is evaluated numerically for different coolants employing three flow rates (17 g/s, 34 g/s and 50 g/s). Hence, the effects of fin height, spacing and thickness, and mass flow rate on the overall heat transfer coefficient (CHT) and pressure drop (ΔP) are reported for the abovementioned coolants. It is found that increasing the mass flow rate increases both the CHT and ΔP . It is also noted that increasing the fin height and spacing decreases both the CHT and ΔP , as opposed to increasing the thickness, which causes both the CHT and ΔP to increase. Among the three coolants used, the sCO₂ shows superior performance compared to the water and nanofluid and this based on higher CHT and lower ΔP . Moreover, the performance evaluation criterion (PEC) for the sCO₂ is higher than that for the water and nanofluid by 53% at 17 g/s flow rate and 243% at 50 g/s flow rate.

Keywords: heat transfer; mini-channel heat sink; supercritical carbon dioxide; nanofluid; microelectronic cooling



Citation: Alemam, A.; Yehya, S.A.; Omer, A.S.; Hamza, A.; Saeed, M.; Berrouk, A.S. Performance Comparison of Mini-Rectangular Fin Heat Sinks Using Different Coolants: Supercritical CO₂, Water and Al₂O₃/H₂O Nanofluid. *Energies* **2022**, *15*, 8734. <https://doi.org/10.3390/en15228734>

Academic Editor: Gabriela Humnic

Received: 29 September 2022

Accepted: 7 November 2022

Published: 20 November 2022

Publisher's Note: MDPI stays neutral with regard to jurisdictional claims in published maps and institutional affiliations.



Copyright: © 2022 by the authors. Licensee MDPI, Basel, Switzerland. This article is an open access article distributed under the terms and conditions of the Creative Commons Attribution (CC BY) license (<https://creativecommons.org/licenses/by/4.0/>).

1. Introduction

With the advancement of microelectronic devices, the need for digital thermal management is rising. These microdevices are performing heavy tasks that cause them to produce high heat fluxes and subject the systems to performance deficiency, signal noises and even complete failure [1]. Continuous removal of dissipated heat is required to maintain the devices working properly. Micro and mini channel heat sinks can extract dissipated heat from the electronic devices with the high cost of external pumping requirements. Efforts are being made to enhance heat sinks' thermal and hydraulic performance using optimized heat transfer techniques. The various cooling methods investigated so far include changing the shape of the channel, increasing surface roughness, creating cavities on the walls and using nanofluids in the base fluid. Air cooling is favored because of its simple design, but is usually limited to low heat-fluxing systems [2]. However, liquid-cooling systems are preferred in high heat-fluxing systems due to their high convection rate, but their design complexity and cost are increased compared to air-cooled systems [3]. Using nanofluids

has gained substantial attention owing to their ability to increase the thermal conductivity of the coolant and hence increase heat transfer rate.

Computational fluid dynamics (CFD) packages have helped analyze the thermal and hydraulic performance of micro and mini channel heat sinks. The performance of heatsinks is usually optimized in terms of geometry and coolant to decrease the need for high pumping power due to their small sizes. In terms of optimizing the geometry of the heat sink, Li and Peterson [4] simulated a 3D heat sink model to optimize the heat transfer performance of a silicon-based heat sink for a constant pumping power of 0.05 W. The optimal dimensions were found to be 100 μm (pitch), 60 μm (width) and 700 μm (depth), respectively. Lei et al. [5] investigated the thermal performance of microchannel heat sinks with periodic expansion–constriction cross-sections experimentally and numerically. They examined the conjugate heat transfer, entrance effect, multi-channel effect, viscous heating and effect of temperature-dependent properties. The friction factor and Nusselt number obtained from the model agreed with the experimental results. Zhang et al. [6] optimized the heat sink geometry by introducing the fins configuration (structure parameters and different arrangements) in the straight channel.

The pressure drop of the optimized model was reduced by 13.33% compared to the straight channel geometry. Kumar and Singh [7] numerically investigated different flow arrangements for uniform and non-uniform (hot spots) temperature distributions. Aliabadi et al. [8] investigated the sinusoidal-wavy mini-channel heat sink and analyzed cooling performance for different wavelength and wave amplitude geometrical parameters. It was found that sinusoidal channels provide higher thermal efficiency and pressure drop than straight channels, and they have an optimum combination of wavelength and amplitude values that produce a high heat flux to pumping power ratio. Khoshvaght-Aliabadi and Feizabadi [9] found that the pumping power is higher in sinusoidal channels with straight fins than in straight channels with sinusoidal fins, but the former produces better temperature uniformity and lower base temperature than the latter. Lei Chai et al. [10] simulated the thermal performance of a microchannel heat sink with triangular ribs and investigated the different geometry arrangements. Thermohydraulic performance was found to be highly dependent upon the rib geometry. Bello-Ochende et al. [11] simulated the 3D heat sink model and investigated the cross-sectional aspect ratio to optimize the geometry for a constant value of solid volume fraction. The pressure drop was found to be increased by increasing the optimal aspect ratio. Liang Gong et al. [12] numerically examined the influence of wavy channels, wavelength, and amplitude on the thermal performance of microchannel heat sinks for Reynolds number between 50 and 150. The performance of wavy channels heat sink was found to be 55% improved as compared to the straight channel heat sink. Wang et al. [13] used the inverse problem method to optimize the microchannel heat sink geometry using a multi-parameter optimization approach. The effectiveness of the heat sink was found to be decreased with increasing pumping power. Caney et al. [14] investigated the heat transfer frictional pressure drop of single phase in a microchannel heat sink and confirmed the accuracy of classical correlations used for conventional size channels. Tullius et al. [15] conducted numerical studies and optimized the pin fin geometry considering the material and dimensions of the fin. Xie et al. [16] performed the simulations to observe the influence of inlet velocity, bottom wall thickness and channel wall thickness on the pressure drop and thermal characteristics of heat sink. Heat transfer and pressure drop were found to be increased by increasing the depth of channels and reducing the channels gap. Naphon et al. [17] enhanced the heat removing potential of the mini-channel by introducing a liquid impingement approach. Panao et al. [18] introduced an intermediate jet spray system to enhance liquid jet cooling. Hu et al. [19] experimentally studied the mass flow rate of water passing through the sink and air inlet velocity in the heat exchanger for a real scenario of a CPU. Wang et al. [20] considered a variation in thermophysical properties with temperature and optimized the heat sink geometry for pumping power, inlet volume flow rate and pressure drop.

In terms of using coolants in mini channel heat sinks, Peyghambarzadeh et al. [21] experimentally investigated the performance of CuO and Al₂O₃-based nanofluids in rectangular microchannels; 1 vol.% Al₂O₃ and 0.2 vol.% CuO increased the heat transfer coefficient by 49% and 27%, respectively. Roberts and Walker [22] employed nanofluids in the base fluid to enhance the thermal performance of heat sinks. The thermal performance was enhanced by almost 20% by employing Al₂O₃-water nanofluid. Rafati et al. [23] investigated the different concentrations of Al₂O₃, SiO₂ and TiO₂ on the thermal performance of a quad-core processor. Al₂O₃ was the best candidate, resulting in the lowest operating temperature among the nanofluids investigated. Jajja et al. [24] considered a commercial cooling kit and investigated the influence of heat transfer coefficient, thermal resistance and fin spacing on base temperature. The minimum operating temperature was achieved at a volume flow rate of 1.5 L/min in fin spacing of 0.2 mm. Ho et al. [25] employed microencapsulated phase change material (MEPCM) particles in pure water to enhance the thermal performance of mini channel heat sink. They evaluated the thermal and hydraulic characteristics for the Reynolds number ranging from 133 to 1515. (MEPCM) based fluid with the lower mass flow than water exhibited higher thermal performance. Naphon et al. [26] investigated the TiO₂ nanofluids in deionized water and analyzed the effect of nanofluid inlet temperature, heat flux and Reynolds number on the thermal characteristics of the rectangular fin heat sinks. Ijam et al. [27] employed Al₂O₃ and TiO₂-based nanofluids in a copper mini-channel heat sink. Cooling performance was found to be enhanced by 2.95% to 17.32% and 1.88% to 16.53% for the Al₂O₃-water and TiO₂-water fluids, respectively. Rimbault et al. [28] analyzed the thermal and hydraulic characteristics of CuO nanoparticle-water nanofluid inside a rectangular microchannel heat sink experimentally. Low particle volume nanofluids (0.24% and 1.03%) exhibited a small heat transfer enhancement, while high particle volume (4.5%) fraction showed a decrement in the heat transfer. Moraveji et al. [29] numerically investigated the cooling performance and pressure drop of the heat sink using the TiO₂ and SiC nanoparticles. The heat transfer coefficient was found to be increased with the increase in the volume fraction of particles. Afrand [30] investigated the effect of nanoparticle MgO on the thermal conductivity of base fluid ethylene glycol experimentally. The thermal conductivity of ethylene glycol was found to be increased with the increase in volume concentration of MgO nanoparticles. Dominic et al. [31] compared the performance of two coolants, deionized water and Al₂O₃/water nanofluid in sinusoidal heatsinks. They found that although the nanofluid had a higher heat transfer coefficient, it still yielded a weaker performance than deionized water, mainly due to its lowered specific heat and increased pressure drop. Babar et al. [32] experimentally investigated the staggered airfoil fin shape heat sink using the novel ferric oxide- (Fe₂O₃) and silica (SiO₂)-based water nanofluids at different mixing ratios. They reported a maximum enhancement of 17.65% in the heat transfer coefficient against the heating load of 75 W. Ambreen et al. [32] analyzed the thermal performance of pin fin heat sink using the MXene-based nanofluid (Ti₃C₂T_x) using both numerical and experimental techniques. The maximum enhancement of 40.5% in the average Nusselt number was found for the nanofluid concentration of 0.027 vol.%. Saed et al. [33] considered the porous substrates in horizontal and vertical direction to investigate the heat transfer and hydrodynamic characteristics of alumina-water nanofluid in microchannel heat sink. They reported that material of porous substrate and heat sink greatly affect the CPU average temperature and the overall thermal resistance. Hossain Nemaiti [34] employed entropy generation minimization method and developed some dimensionless form of equation to optimize the plate fin heat sink. He proposed a semi-analytical relation which relates different dimensionless parameters. Chai et al. [35] investigated the performance of the addition of nanoparticles of PCMs in a base fluid. They found that due to the latent heat provided by the PCM, it yielded a higher specific heat and heat transfer coefficient than the base fluid, but it achieved overall weaker performance due to the increased viscosity and pressure drop. Saeed et al. [36] analyzed mini-channel heat sinks for different geometry configurations and two different volume concentrations of Al₂O₃/H₂O nanofluid. Results

depicted a higher heat transfer coefficient for nanofluids as compared to distilled water. Fronk and Rattner [37] compared the use of fluids at supercritical state. These fluids were single-phased (water and FC-72), two-phased (boiling R134a) and CO₂. They found that the supercritical CO₂ (sCO₂) achieved lower wall temperature than the single-phased coolants and required less pumping power due its risen volumetric thermal capacity. Moreover, the results of Saeed et al. [3] showed that sCO₂ achieved a seven-times reduced pressure drop and enhanced cooling performance by 32% than water at a higher flowrate of coolants in mini-channels. Awais et al. [11] found that the performance of sCO₂ is double that of water at 8 MPa inlet pressure and that the pressure drop is reduced by 60.65% and 62.41% at inlet pressures of 10 and 12 MPa, respectively. Jung et al. [38] experimentally investigated the velocity and temperature fields of Al₂O₃ nanofluid in microchannel heat sink using the laser induced fluorescence and particle image velocimetry techniques. Nanofluid exhibited the lesser generation rate of thermal entropy as compared to water. Bahiraei et al. [39] investigated the second law characteristics of microchannel heat sink using the different shapes of nanofluids at different Reynolds numbers. Frictional entropy generation was found to be increased while thermal entropy generation diminished at a high Reynolds number. Yan et al. [40] analyzed the heat transfer coefficient of Al₂O₃-water nanofluid numerically using the micro-encapsulated phase change material as the ceiling of the heat sink. Nanoparticles with a solid volume fraction of 10% exhibited a decrease in thermal resistance by 10.88% in the case of bare ceilings. Ho et al. [41] experimentally analyzed the transient thermal characteristics of mini channel heat sink with micro-encapsulated phase change material (MEPCM) in its ceiling using the Al₂O₃/water nanofluid. The addition of nanofluid resulted in a decrement of MEPCM layer temperature and wall temperature. As seen from the abovementioned investigations, the previous studies report the performance of mini-channel heat sinks using individual fluids only, mostly water or nanofluids. However, the poor hydraulic performance linked with these coolants, coolant leakage and channel collaging issues entail the need to investigate new coolants capable of eluding formerly mentioned complications. In this reference, supercritical CO₂ can be a good substitute for water and nanofluids with its excellent thermal and hydraulic characteristics (here, we need to cite our PCHE papers and heat sink paper). Further, it operates in the gas phase, so its accidental leakage will not damage the electronic devices. Hence, this study aims to analyze the potential of sCO₂ as a coolant for mini-channel heat sinks and compare its thermohydraulic characteristics with the previously used coolants (water and nanofluids). Further, the influence of geometry variation of the heat sink on the thermal and hydraulic characteristics of the mini channel heat sink is also investigated and compared for these three coolants, i.e., CO₂, water and Al₂O₃/H₂O. The comparative analysis of these three coolants on the performance parameters of mini channel heat sinks will add innovation to the literature and help the researchers optimize the design and performance of heat sinks in future.

As seen from the abovementioned investigations, the previous studies report the performance of mini-channel heat sinks using individual fluids only, mostly water or nanofluids. However, the poor hydraulic performance linked with these coolants, coolant leakage and channel collaging issues entail the need to investigate new coolants capable of mitigating these complications. In this regard, supercritical CO₂ can be a good substitute for water and nanofluids thanks to its excellent thermal and hydraulic characteristics. Further, it operates in the gas phase, so its accidental leakage will not damage the electronic devices. Based on the above, this study aims to analyze the potential of sCO₂ as a coolant for mini-channel heat sinks and compare its thermohydraulic characteristics with the previously used coolants (water and nanofluids). The influence of many design parameters on the thermal and hydraulic characteristics of the mini channel heat sink is also investigated and compared for these three coolants, i.e., sCO₂, water and Al₂O₃/H₂O. The comparative analysis of these three coolants on the performance parameters of mini channel heat sinks should help the design innovation and optimization of heat sinks used for important applications, such as microelectronic cooling.

2. Case Study and Numerical Model

This study will focus on the flow of three fluids: water, $s\text{CO}_2$ and $\text{Al}_2\text{O}_3/\text{water}$ nanofluid in a single mini-channel. The heatsink dimensions suggested by Awais et al. [11] (see Figure 1) were adopted in this work with 45 mm length, 55 mm width and 6 mm height, and is assumed to be made of copper. This heatsink was designed to be used to dissipate heat generated by an electronic device with power of 325 W.

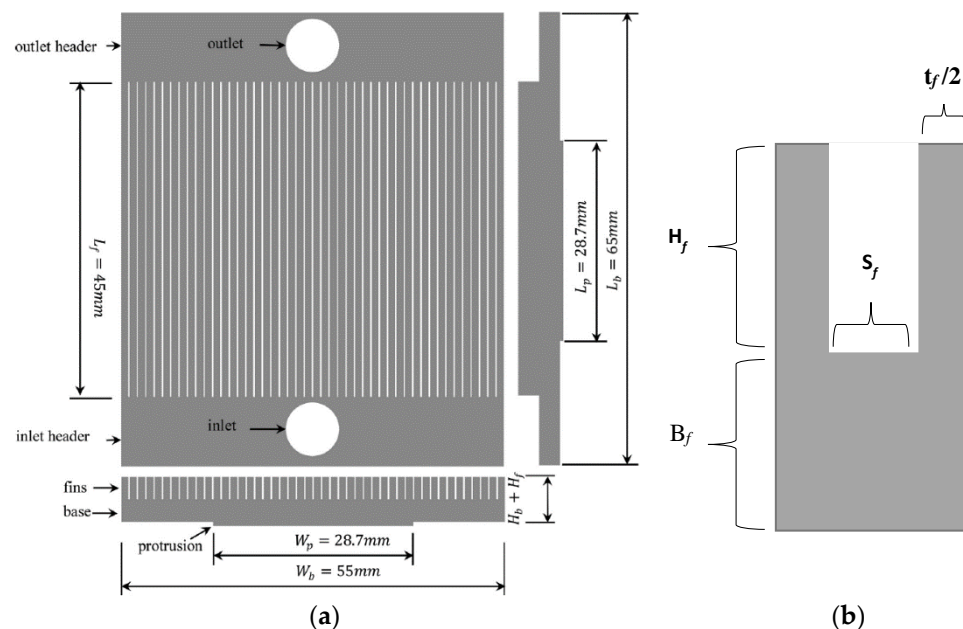


Figure 1. (a) Schematic of the entire heatsink [11]; (b) a single mini-channel.

Moreover, it is comprised of several mini-channels with a rectangular cross-section, and the flow rate is considered to be uniformly distributed across the mini-channels inlet. The inlet conditions of the fluids are 25 °C and 1 atm for the water and nanofluid, while for the $s\text{CO}_2$, they are set to the temperature and pressure that achieve the maximum heat transfer coefficient, which is 34 °C and 8 MPa, respectively. The flow rates were divided by the number of channels for every simulation. Table 1 describes the specifications of the case study, which results in 36 different geometries with a total number of 108 simulations.

Table 1. Specifications of the case study.

Fin thickness t_f (mm)	0.5 and 1
Fin spacing S_f (mm)	0.5 and 1
Fin height H_f (mm)	2, 3 and 4
Fin length L_f (mm)	45
Number of channels	28, 37 and 55
Mass flowrates (g/s)	17, 33 and 50

2.1. Numerical Model

The fluid and solid domains were solved by utilizing the steady form of the Navier-stokes equation. The case study was based on the following assumptions: (1) neglecting the gravitational forces on the fluid, (2) the top wall of the channel is insulated, (3) the contact resistance between the heat source and the channel base is neglected. In the fluid domain, the equations are incompressible for the water and nanofluid and compressible for the $s\text{CO}_2$ and comprising of the mass continuity Equation (1), the momentum Equation (2),

the total energy Equation (3) for the sCO₂ and the thermal energy equation for the water Equation (4) [3].

$$\nabla \cdot (\rho \mathbf{u}) = 0 \quad (1)$$

$$\nabla \cdot (\rho \mathbf{u} \otimes \mathbf{u}) = -\nabla p + \nabla \cdot \boldsymbol{\tau} \quad (2)$$

$$\nabla \cdot (\rho \mathbf{u} h_{\text{tot}}) = \nabla \cdot (\lambda \nabla T) + \nabla \cdot (\mathbf{u} \cdot \boldsymbol{\tau}) \quad (3)$$

$$k \nabla^2 T = \rho c_p (\mathbf{u} \cdot \nabla T) \quad (4)$$

For the nanofluid, a single-phase model was used consisting of the continuity equation (Equation (5)) with the effective density of the nanofluid described in Equation (6), where ϕ represents the volume fraction of the phase and subscripts n and k, denote the index of the phase and the total number of phases (liquid water and solid nanoparticles) in the nanofluid mixture, respectively. Additionally, the momentum equation (Equation (7)) and the effective viscosity equation (Equation (8)) are aforementioned [36].

$$\nabla \cdot (\mathbf{u}_m) = 0 \quad (5)$$

$$\rho_{\text{eff}} = \phi \rho_p + (1 - \phi) \rho_{fl} \quad (6)$$

$$\nabla \cdot (\rho_{\text{eff}} \mathbf{u}_m \mathbf{u}_m) = -\nabla p + \nabla p + \nabla \cdot [\mu_{\text{eff}} (\nabla \mathbf{u}_m + \nabla \mathbf{u}_m^T)] \quad (7)$$

$$\mu_{\text{eff}} = (1 + 7.3\phi + 123\phi^2) \mu_{Al} \quad (8)$$

Additionally, the energy equation is represented in Equation (9), and Equation (10) was utilized to attain the effective thermal conductivity of the nanofluid with d_{fl} , K_{fl} , d_p and K_s denoting the diameter of particulate and thermal conductivity for the fluid and solid phases, respectively. Moreover, to obtain the Prandtl and Reynolds numbers Equation (11a–c) were used, where B_c is the Boltzman constant ($1.3807 \times 10^{23} \text{ JK}^{-1}$) and l_{BF} is the mean free path for water. Additionally, the energy equation for the solid domain is represented in Equation (12) [36,42].

$$\nabla \cdot (\rho_{\text{eff}} C p_{\text{eff}} \mathbf{u}_m T) = k_{\text{eff}} \nabla^2 T \quad (9)$$

$$\frac{K_{\text{eff}}}{K_{fl}} = 1 + 64.7\phi^{0.7460} \left(\frac{d_{fl}}{d_p}\right)^{0.369} \left(\frac{K_s}{K_{fl}}\right)^{0.7476} \text{Pr}^{0.9955} \text{Re}^{1.2321} \quad (10)$$

$$(\rho C p)_{nf} = (1 - \phi)(\rho C p)_{fl} + \phi(\rho C p)_s$$

$$\text{Pr} = \frac{C p_{nf} \mu}{K_{\text{eff}}} \quad (11a)$$

$$\text{Re} = \frac{\rho_f B_c T}{3\pi \mu^2 l_{BF}} \quad (11b)$$

$$\mu = A \times 10^{\frac{B}{1-C}} \quad \text{where} \quad C = 140, V = 247 \text{ and } A = 2.414e^{-5} \quad (11c)$$

$$k_{\text{solid}} \nabla^2 T = 0 \quad (12)$$

The ANSYS CFX solver is based on the vertex-centered finite volume method to discretize the fluid and solid domains. The control volume compounds the smaller volumes neighboring the vertex. All the variables are stored per vertex. The pressure-velocity coupling is achieved by the Rhie-Chow algorithm. Moreover, the solver utilizes a blend of the second and first-order unwinding schemes to achieve higher accuracy. As opposed to just using the first-order scheme, this blend preserves boundedness and limits the numerical diffusion, but it will result in a looser and slower convergence.

The model consists of the fluid domain, the solid domain and interfaces. The volume fraction of the solid phase in the nanofluid is set at 2.5%. Two types of interfaces are defined,

the fluid-solid interface in the channel and a solid-solid interface at the outside vertical walls of the fins to achieve periodicity of the neighboring channels. Equation (13a–c) states the governing conditions at the interfaces. The fluid domain is set at a reference pressure equaling 8 MPa for the sCO₂ and 1 atm outlet pressure for water and nanofluid. Moreover, the inlet boundary conditions are set to the inlet static temperatures and mass flow rates per channel. Additionally, the upper channel wall is set to be adiabatic as presented in Equation (14), while the base of the channel is designed to have a continuous heat flux equaling to Equation (15).

$$V = 0 \quad (13a)$$

$$T_{Solid} = T_{fl} \quad (13b)$$

$$k_{solid} \frac{\partial T_{Solid}}{\partial S_n} = k_{fluid} \frac{\partial T_{fl}}{\partial S_n} \quad (13c)$$

$$\frac{\partial T_{Solid}}{\partial S_n} = 0 \quad (14)$$

$$\dot{q}_b = -\frac{k \partial T_{solid}}{\partial S_n} = -\frac{325}{A_{base}} \quad (15)$$

For the water and nanofluid, the laminar flow model is utilized. At the same time, for the sCO₂ it is critical to select the appropriate turbulence model to enhance the accuracy in calculating the boundary layer thickness. The shear stress model (SST) is found to be suitable to calculate the thermohydraulic characteristics of the flow near the boundary layer. It provides ascending performance when it comes to predicting the separation from a surface due to adverse pressure gradient conditions. Moreover, it combines the K- ω and the K- ϵ turbulence models by utilizing the former in the regions near the wall and the latter for the rest of the flow. Furthermore, the SST calculates the turbulent eddy viscosity term (μ_T) from the kinetic energy and frequency of the turbulence as presented in Equation (16) [43].

$$\mu_T = \rho k / \omega \quad (16)$$

The properties of carbon dioxide change severely at the critical point. In order to account for said changes in the ANSYS CFX, a high-resolution real gas property (RGP) table was uploaded in the solver. The RGP table consists of 400 pressure values ranging from 7.98 to 8.02 MPa and 600 temperature values ranging from 300 to 360 K. The RGP file was coded with MATLAB and NIST's REFPROP. Furthermore, its accuracy was proven in the previous work of Awais et al. [11] by comparing the density variations along the channel length from the CFX solver with that from the NIST's REFPROP.

To account for the thermo-hydraulic properties of the case study, the following expressions are evaluated in the CFX post-processor. The total heat flux through the fluid-solid interface Equation (17), the log-mean temperature difference (LMTD) Equation (18) and the overall heat transfer coefficient (U) Equation (19).

$$\dot{q}_i = \frac{1}{A_i} \int_{A_i} \varphi_{cf} \quad (17)$$

$$LMTD = \frac{(T_b - T_i) - (T_b - T_o)}{\ln((T_b - T_i)/(T_b - T_o))} \quad (18)$$

$$U = \dot{q}_i / LMTD \quad (19)$$

where A_i , and φ_{cf} represent the area of the fluid-solid interface and the heat flux through the cell-face, respectively. Additionally, T_b , T_i and T_o correspond to the average temperatures at the base, inlet and outlet, respectively.

2.2. Mesh Optimization

The ANSYS-ICEM mesh generator was utilized to construct hexahedral elements by creating structured blocks for the domains. A 1:1 nodal association at the interface between the domains is maintained through the assurance of identical topology. In order to achieve the optimum mesh design, four meshes (M1, M2, M3 and M4) were investigated for the sCO₂ simulations by monitoring the values of \bar{T}_{Base} , pressure drop across the channel length (ΔP) and the U. The mesh optimization study was conducted on the simulation case with the highest Reynolds number (i.e., lowest S_f and highest flowrate). At the smaller-sized meshes M3 and M4, the T_b varied by 0.1%, The ΔP by 1.2% and the U by 0.8%. The memory allocated for M4 is 54% higher than that allocated for the M3. Moreover, the computational time is 62% higher for the M4. Hence, the M3 posed the optimum choice for higher accuracy with less computational time. Table 2 depicts the investigated meshes.

Table 2. Mesh independence study of a mini-channel with t_f and S_f equaling 0.5 and 1 mm, respectively.

	M1	M2	M3	M4
NE along S_f	15	30	40	50
NE along L_f	60	85	100	120
NE along H_f	20	35	45	55
No. of nodes	111,300	291,550	473,000	747,600
T_b (°C)	44.92	44.85	44.81	44.77
ΔP (kpa)	8.47	9.07	9.27	9.38
U (W/m ² K)	3716.3	3818.32	3849.82	3881.99
Space on disk (MB)	182.19	359.1	559.97	863.98
CPU time/iteration (s)	0.81	3.38	6.42	10.38

In order to maximize the effectiveness of the SST model, the values of the y_+ were maintained below 1. That was achieved by ensuring the distance of the first node to be equal to 5×10^{-7} mm and the growth rate to be equal to 1.1. The final mesh is presented in Figure 2 where the green and blue regions represent the fluid and solid domains, respectively.

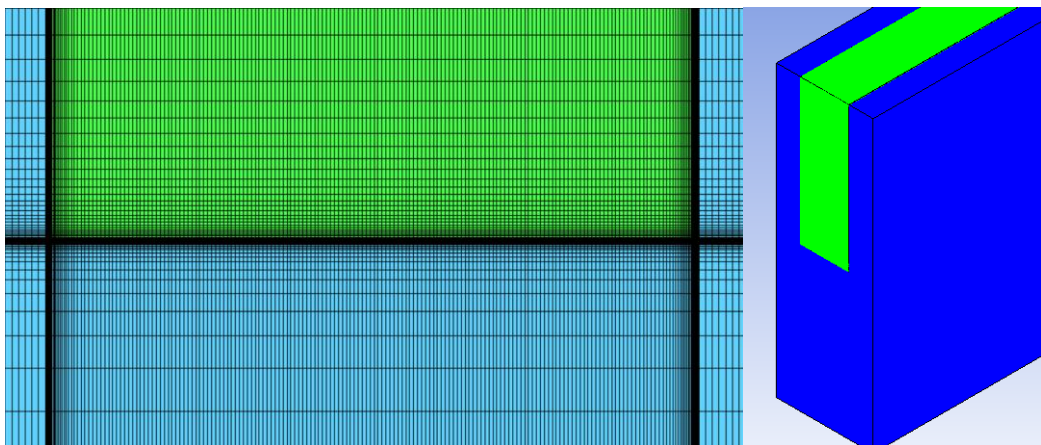


Figure 2. A closeup of the final mesh with first node distance 5×10^{-7} mm and inflation rate 1.1.

2.3. Model Validation

Validation for coolant water

For the purpose of investigating the validity of the current model, the difference between the pressure drop (ΔP) per channel for the water simulations with t_f , S_f and height equaling 1, 1 and 3 mm, respectively, at different flow rates are compared with those obtained from the work of Saeed and Kim [44]. Figure 3a depicts the trends of ΔP for the work of Saeed and Kim and the current. As shown in the figure, the ΔP for the current work follows a similar trend to the Saeed and Kim's work. However, the differences in magnitude between both works range from 8 to 12%. The reason behind the change could be attributed to the fact that the trend of Saeed and Kim corresponds to the averaged values for the total number of channels.

Validation for coolant CO₂

The numerical model developed for sCO₂-cooled microchannel heat sink geometry is validated using the experimental study of Huai et al. The test section is shown in Figure 3b that involves 10 circular channels. For the validation purpose, the dimensions of the computational domain employed are 2 mm × 2 mm × 500 mm and are shown in Figure 3b. A 9-kW heat flux was applied on the top and bottom surfaces (Figure 3a). The topology of mesh generated that consist of two O-grids (O1 and O2), node distribution and mesh itself is shown in the same figure. The comparison of the computed results and experimental results is shown in Figure 3c,d. The comparison of the results shows that computed results are well within the acceptable limits of the experimental results and adopted model can be used for the current study. Further details on the validation of the model can be found in the author's previous work [3].

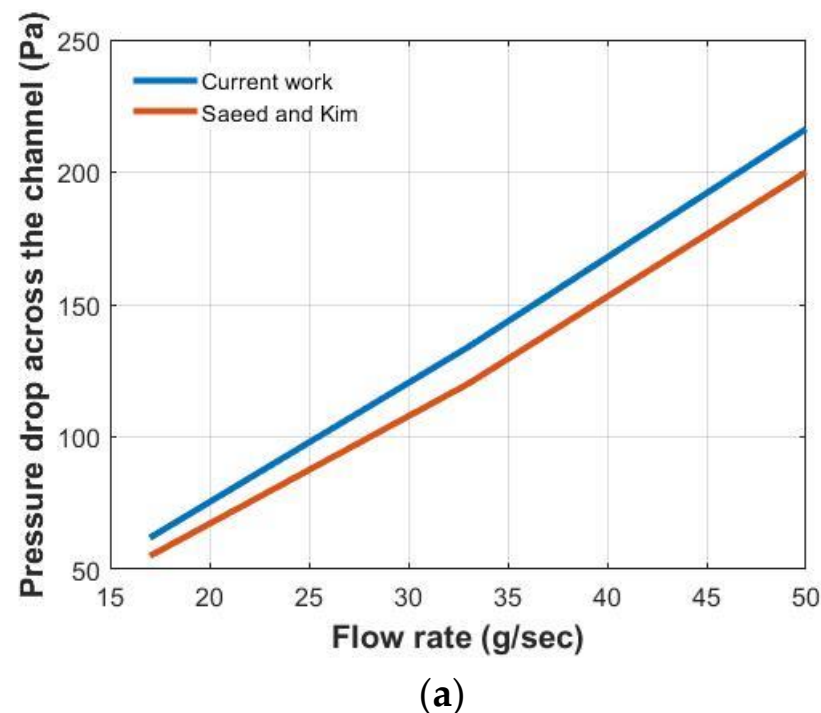


Figure 3. Cont.

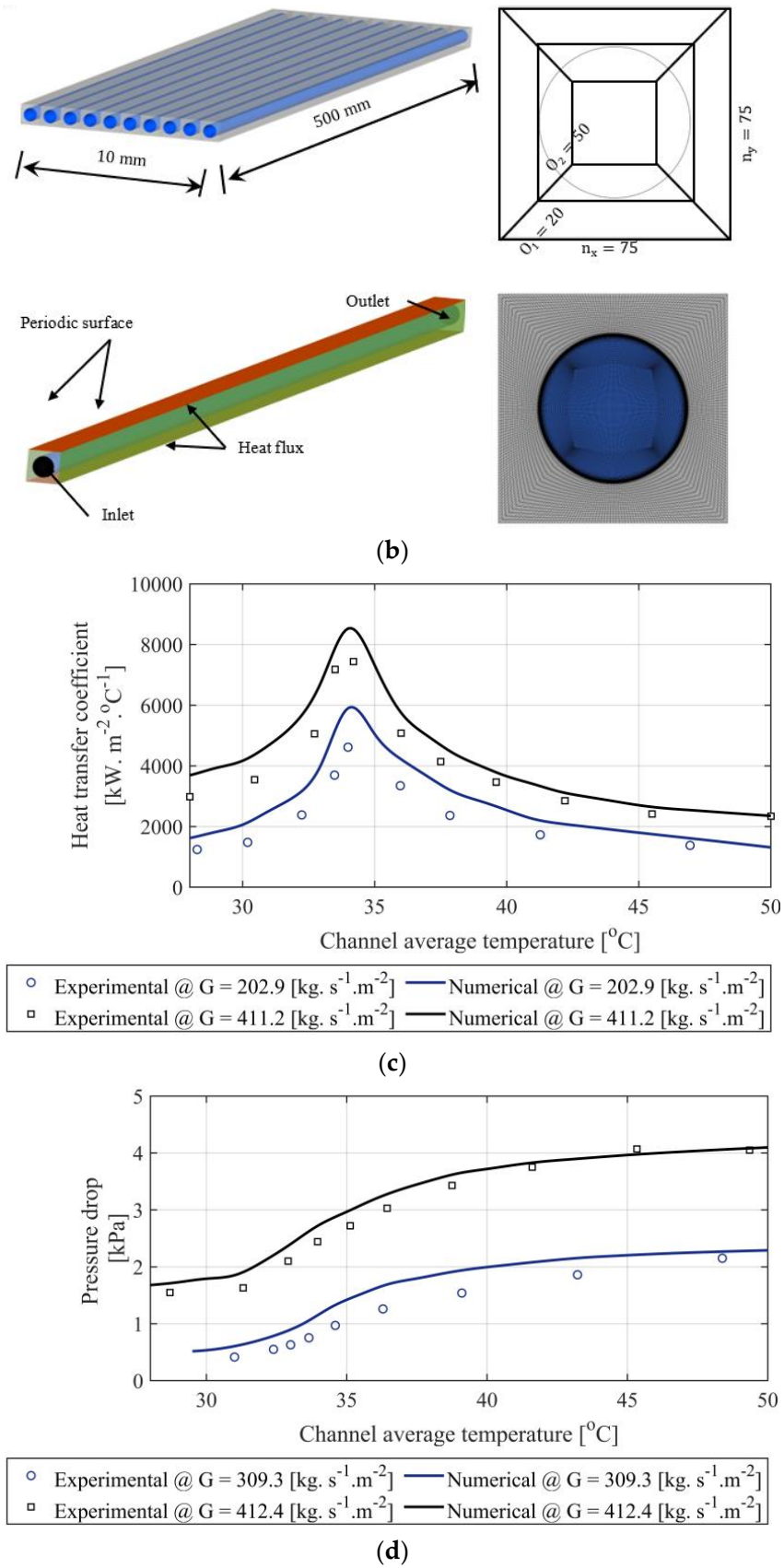


Figure 3. (a) Comparison of pressure drop values of the water of the current work and Saeed and Kim [42], (b) computational domain and mesh, (c) comparison of the heat transfer coefficients [3] (d) comparison of the pressure drop [3].

3. Results and Discussion

The thermohydraulic characteristics of the micro-channel heat sink were investigated in terms of geometry and type of coolant. The effects of changing the channel height, thickness and spacing on the overall heat transfer coefficient of (CHT) and pressure drop (ΔP) were studied for water, $s\text{CO}_2$ and $\text{Al}_2\text{O}_3/\text{water}$ nanofluid.

3.1. Fin Height

The fin height significantly affects the performance of the heat sink, as it is shown in Figures 4 and 5, where the former depicts the effect of fin height on CHT and the later ΔP . Three heights were investigated, namely, 2 mm, 3 mm and 4 mm for 1 mm t_f and 0.5 mm S_f . For the water and nanofluid, Figure 4 shows the CHT declining as the height increases and growing as the mass flow rate increases. This can be attributed to the inverse proportionality of CHT with the overall area of heat transfer. Additionally, because of the high-volume concentration of water in the nanofluid, the CHT values for the water and nanofluid are almost identical, with a maximum of 2% discrepancy. For the $s\text{CO}_2$, the CHT trend behaves unusually at lower flow rates and 3 mm and 4 mm heights, having values for 4 mm height higher than those for 3 mm, as opposed to values at higher flow rates. At the 2 mm height, the $s\text{CO}_2$ reported the highest CHT values compared to other heights and coolants.

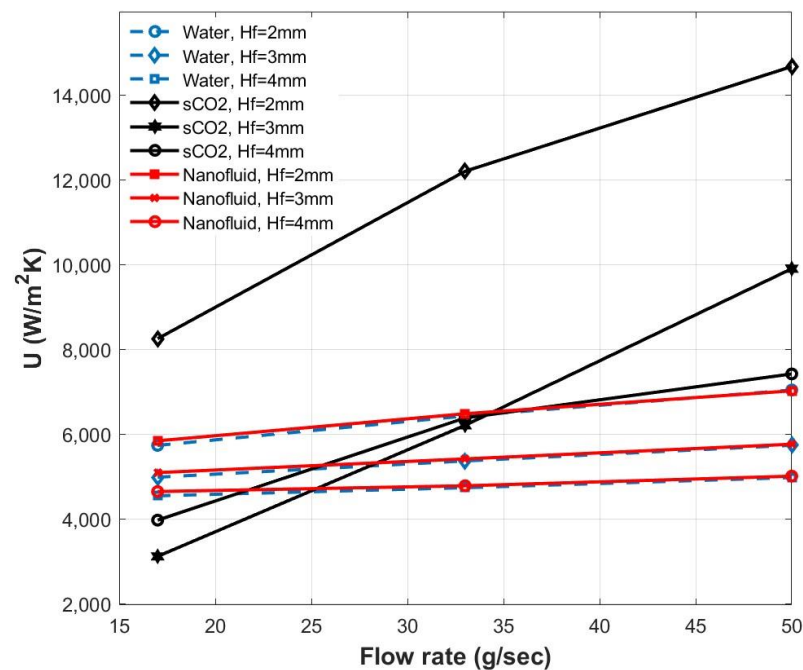


Figure 4. Overall heat transfer coefficient at different flow rates corresponding to different coolants and fin heights.

Figure 5 depicts the effect the fin height has on ΔP for each coolant. It shows the pressure drop increases as the height reduces and grows as the flow rate increases for all coolants. Additionally, the ΔP values for the water and nanofluid are similar, with a maximum discrepancy of 7%. The $s\text{CO}_2$ outperformed the water and the nanofluid with reduced ΔP values. The highest values are reported for the 2 mm height with water or nanofluid acting as coolants, while the lowest values are reported for the 4 mm height with $s\text{CO}_2$ coolant. Overall, this shows that increasing the height has a positive impact in terms of reducing the ΔP and has a negative impact on reducing the CHT.

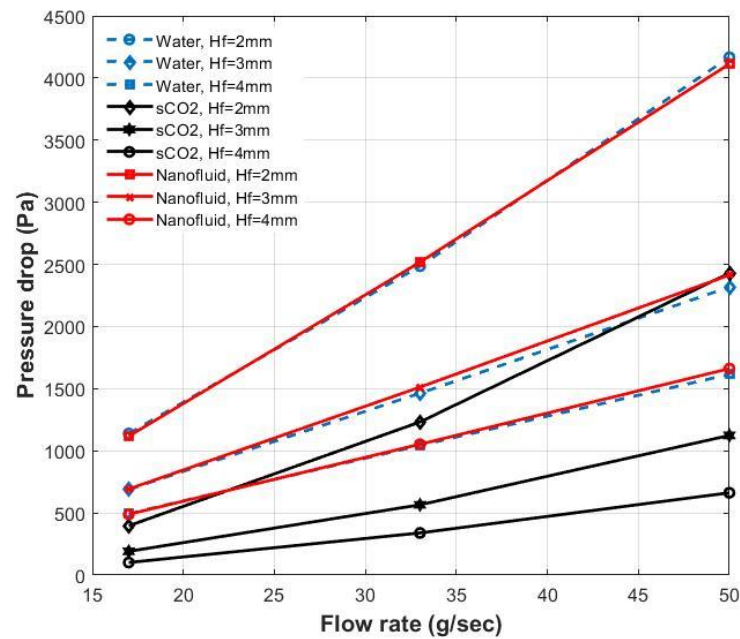


Figure 5. Pressure drops at different flow rates corresponding to different coolants and fin heights.

3.2. Fin Thickness

To study the effect the fin thickness (t_f) has on the heatsink performance, two values were investigated: 0.5 mm and 1 mm, for fixed values of height (H_f) and spacing (S_f) equaling 3 mm and 1 mm, respectively. Figure 6 shows how changing the fin thickness affects the CHT for all coolants. For the water and nanofluid increasing the thickness boosts up the CHT by a seemingly fixed growth as the flow rate increases. Alternatively, for the sCO₂ the effect the thickness has on the CHT increases as the flow rate increases. Consequently, the CHT values of sCO₂ for both thicknesses are lower than those for the water and nanofluid at low flow rates, while at higher flowrate, they supersede those for the water and nonfluid.

Figure 7 shows how the ΔP increases with the thickness at different flow rates for all coolants. It shows the ΔP being higher for the water and nanofluid and the effect the thickness has on the ΔP increasing as the flow rate increases. Moreover, the maximum discrepancy between the ΔP for the water and nanofluid increases from 5% to 8% at the 0.5 mm and 1 mm thicknesses, respectively. The sCO₂ shows lowered ΔP compared to the water and nanofluid, with the 0.5 mm thickness having the lowest ΔP values. Hence, the results indicate that although increasing the fin thickness increases the ΔP , it also increases the CHT as well.

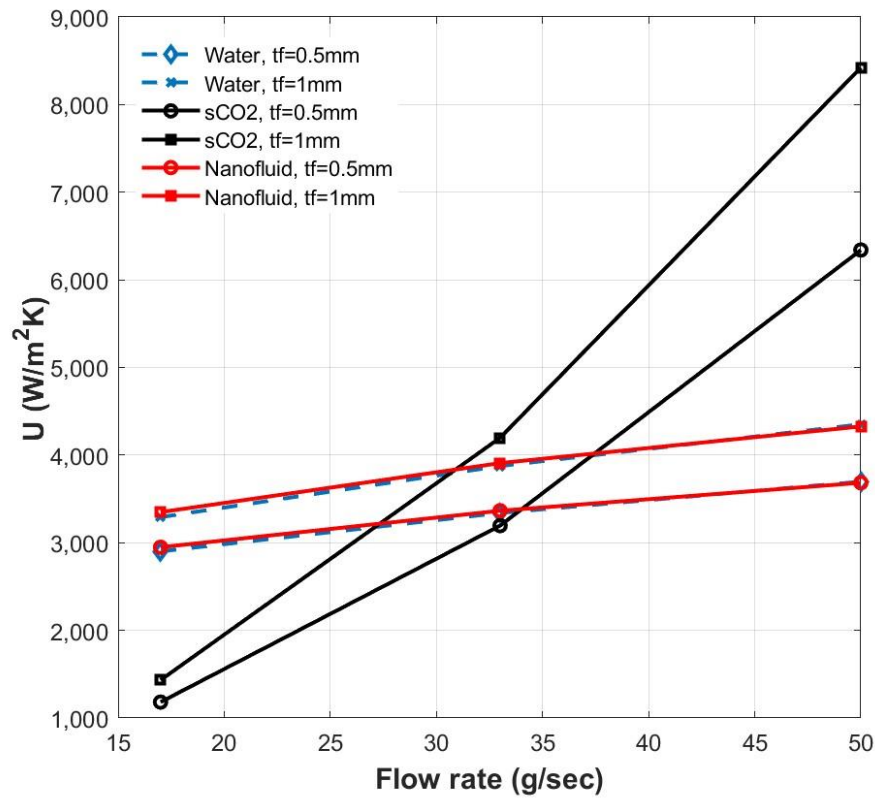


Figure 6. Overall heat transfer coefficient at different flowrates corresponding to different coolants and fin thicknesses.

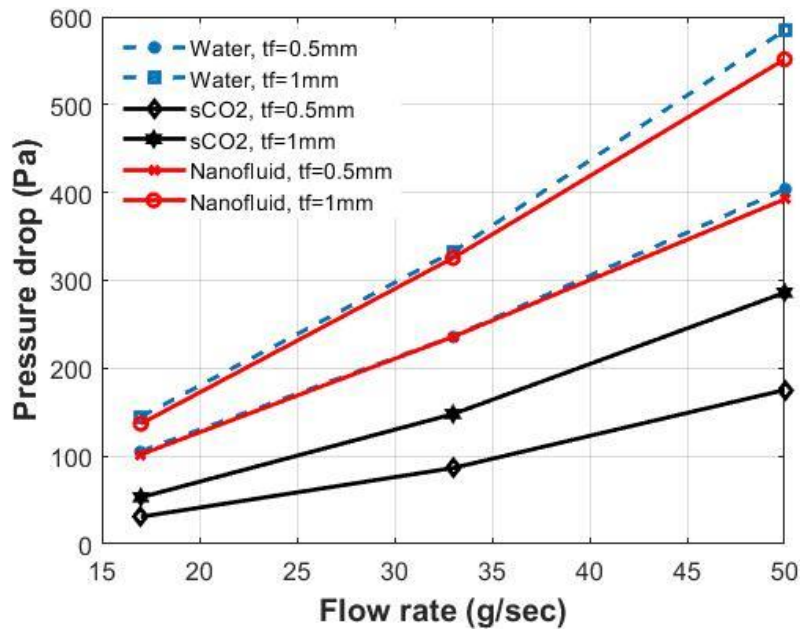


Figure 7. Pressure drop at different flowrates corresponding to different coolants and fin thicknesses.

3.3. Fin Spacing

To investigate the effect of fin spacing (S_f) on the heatsink performance, the spacing was changed from 0.5 mm to 1 mm while maintaining the H_f and t_f at 2 mm and 0.5 mm, respectively. Figure 8a presents the CHT values achieved at the different spacings for all coolants. It shows that increasing the spacing causes the CHT to drop due to the increase in the overall area of heat transfer. The effect of fin spacing on the CHT decreases as the flow rate increases for all coolants. This fact is more noticeable in the sCO_2 trend, which shows

that changing the spacing from 0.5 mm to 1 mm reduces the CHT value by 60% at 17 g/s flow rate and by 7% at 50 g/s flowrates. The highest reported values are for the sCO₂ at 0.5 mm spacing.

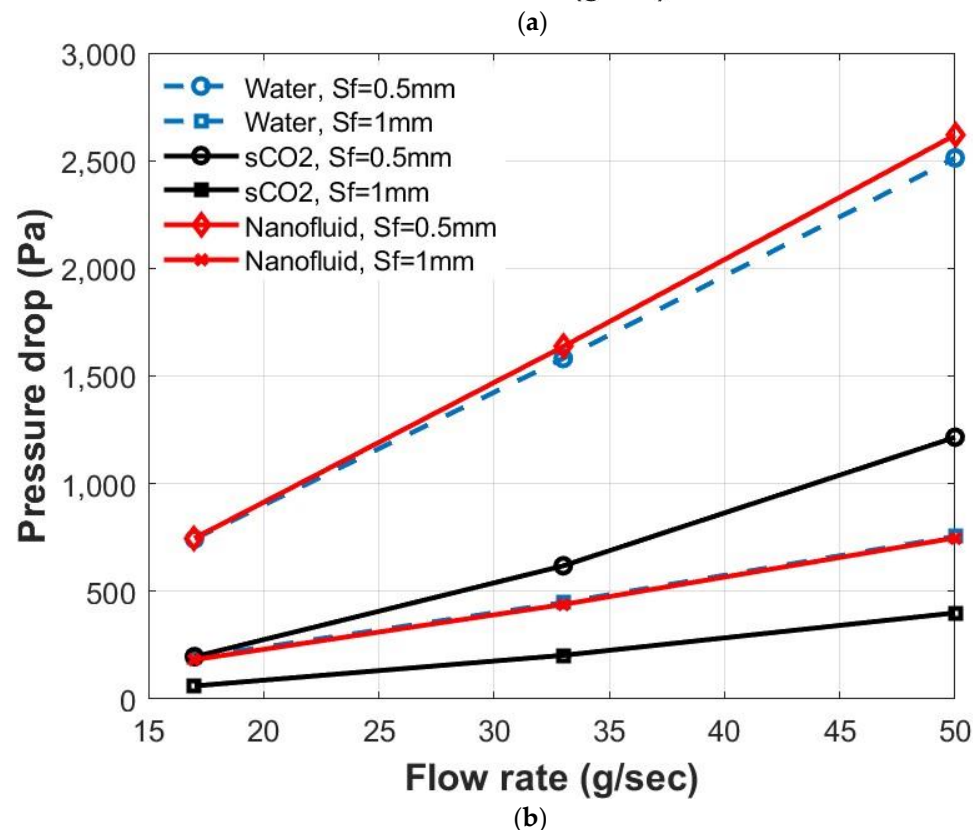
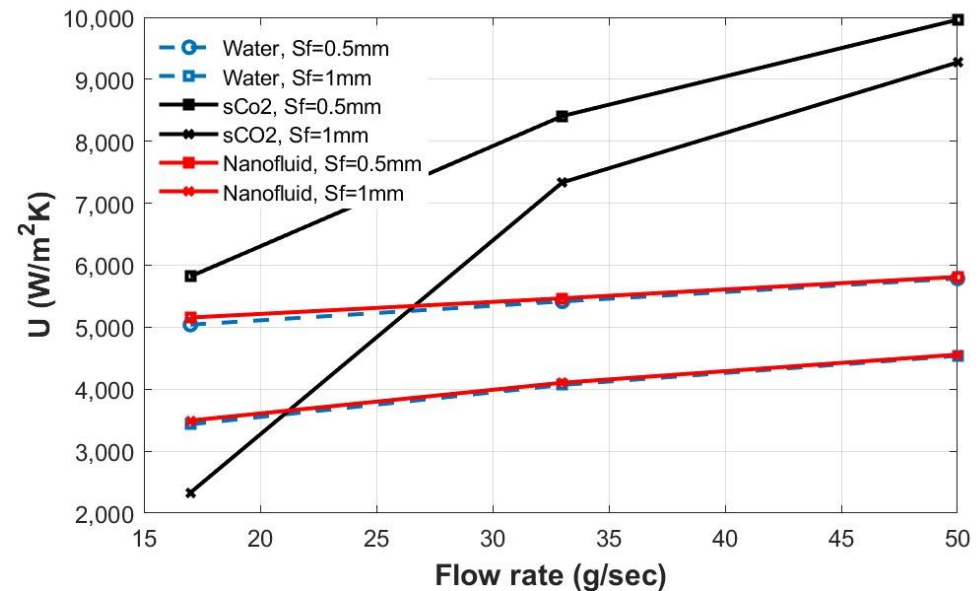


Figure 8. (a) The heat transfer coefficient at different flow rates corresponds to different coolants and fin spacings; (b) pressure drop at different flowrates corresponding to different coolants and fin spacings.

Figure 8b depicts the fin spacing effect on the ΔP at different flow rates for all coolants. It shows that increasing the spacing reduces the ΔP . Moreover, the impact the fin spacing has on the ΔP decreases as the flow rate increases. This phenomenon is more noticeable for the water and nanofluid, with increasing the spacing causing the ΔP to drop by 75% at

17 g/s and by 71% at 50 g/s. The sCO₂ gives the lowest ΔP values at 1 mm fin spacing. In general, much like the fin height, the spacing greatly affects the performance of the heat sink, as it increases both the CHT and ΔP increase.

3.4. Performance Evaluation Criteria (PEC)

The performance evaluation criterion (PER) is a measure of the thermohydraulic performance of heat sinks. It is calculated using Equation (20), where \overline{CHT} and \bar{f} are the averaged values of the overall heat transfer coefficient and friction factor, respectively. The \bar{f} can be obtained by averaging the local values of the f obtained by solving Equation (21). Figure 9 shows the PEC for all coolants at different flowrates for the geometrical configuration of $H_f = 2$ mm, $t_f = 1$ mm and $S_f = 1$ mm. The superiority of the sCO₂ performance is evident compared to the versions of the water and nanofluid, which are almost identical. The sCO₂ outperforms the water and nanofluid by 53% up to 243% as the flow rate increases from 17 to 50 g/s.

$$PEC = \frac{\overline{CHT}}{\bar{f}^{\frac{1}{3}}} \quad (20)$$

$$f = \frac{dp}{dz} \cdot \frac{2}{\rho CHT^2} \cdot D_h \quad (21)$$

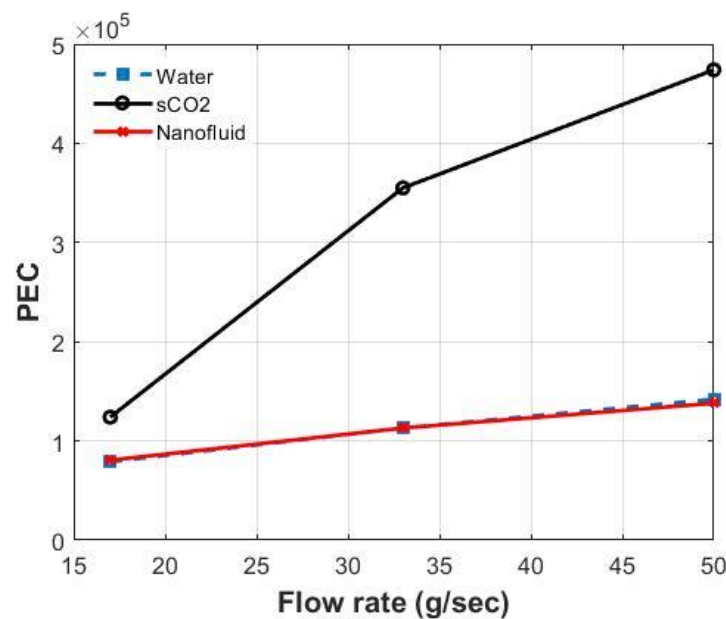


Figure 9. Performance evaluation criteria (PEC) for all coolants corresponding to different flow rates and for $H_f = 2$ mm, $t_f = 1$ mm and $S_f = 1$ mm.

In order to have a comprehensive analysis of the thermophysical properties of sCO₂ as a coolant, the specific heat capacity (C_p) and Prandtl number (Pr) are investigated and presented in Figure 10. The analysis is performed for geometry ($t_f = 0.5$, $S_f = 0.5$ and $H_f = 2$ mm) with variations in the mass flow rate (17 g/s–50 g/s) to study the impact of \dot{m} on C_p and Pr reported in Figure 10. It can be observed from the figure that Pr values increase rapidly along the channel length at lower sCO₂ flow rates until it peaks near the 0.8 of the channel length, after that Pr starts to decrease. In contrast, Pr values vary almost linearly while continuing to increase along the channel length at higher flow rate values. This is also the case for C_p in all studied flow rates scenarios. The maximum C_p and Pr values achieved are 33.5 kJ.g⁻¹ °C and 12.82, respectively in the case of $\dot{m} = 17$ g s⁻¹. Even though the temperature difference between the micro-channels inlet and outlet for the studied geometry and flow rates ranged between 0.3 and 0.7, a significant variation in C_p

and Pr values was detected along the channel's length. This can give an insight into the high thermophysical properties sensitivity of sCO₂ near the critical point.

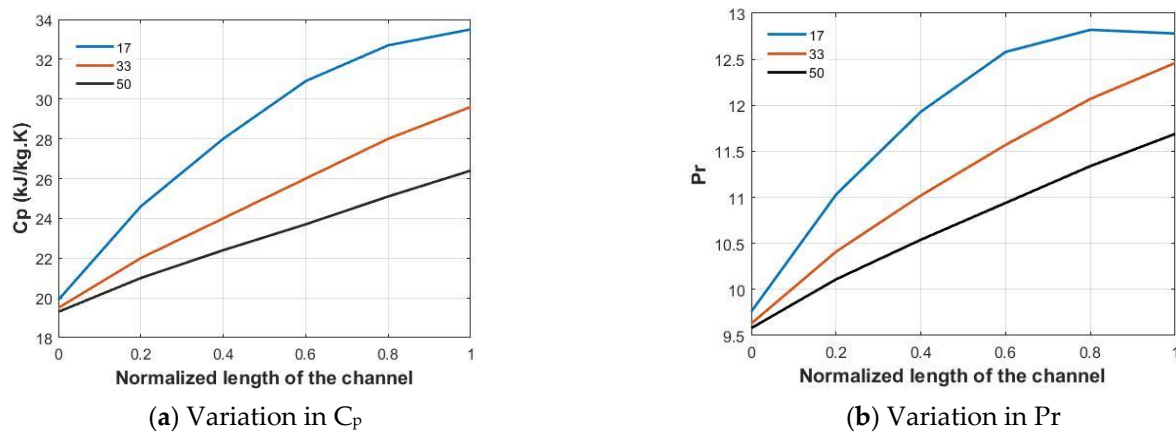


Figure 10. Variation in (a) specific heat capacity and (b) Prandtl number for different sCO₂ mass flow rate with $t_f = 0.5$, $S_f = 0.5$ and $H_f = 2$ mm.

4. Conclusions

The main aim of this work is to investigate the thermohydraulic characteristics of water, nanofluid (Al₂O₃/water), and sCO₂ to be used as coolants in mini-channel heat sinks. The analysis covers three ranges of mass flow rate (i.e., 17 g/s, 33 g/s and 50 g/s) for different fin heights, thicknesses and spacings. After a thorough look into the results, the following conclusions may be drawn.

- For all coolants, increasing the flowrate increases both the overall heat transfer coefficient (CHT) and the pressure drop (ΔP).
- Increasing the fin height and spacing deteriorates the heat sink's thermal performance by reducing the CHT; however, it enhances the hydraulic performance.
- Fin thickness reduction has a beneficial influence on ΔP . Still, its effect on the heat sink's thermal performance is almost negligible compared to the impact of variations in fin spacing and mass flow rate.
- The sCO₂ shows enhanced performance regarding elevated CHT and reduced ΔP compared to the water and nanofluid. Moreover, the performance evaluation criterion (PEC) for the sCO₂ is higher than that for the water and nanofluid by 53% at 17 g/s flowrate and 243% at 50 g/s flowrate.

Author Contributions: Data curation, A.A., S.A.Y., A.S.O., A.H. and M.S.; Formal analysis, M.S. and A.S.B.; Funding acquisition, A.S.B.; Investigation, A.S.B.; Methodology, A.A., S.A.Y., A.S.O. and A.H.; Software, A.A., S.A.Y., A.S.O., A.H. and M.S.; Supervision, M.S. and A.S.B.; Visualization, M.S.; Writing—original draft, M.S.; Writing—review & editing, A.S.B. All authors have read and agreed to the published version of the manuscript.

Funding: The authors acknowledge the financial support from Khalifa University of Science and Technology through the grant No. CIRA-2019-031 and the support from Khalifa University of Science and Technology through the grant No. RC2-2018-024.

Acknowledgments: The authors acknowledge the financial support from Khalifa University of Science and Technology through the grant No. CIRA-2019-031 and the support from Khalifa University of Science and Technology through the grant No. RC2-2018-024.

Conflicts of Interest: The authors declare no conflict of interest.

Nomenclature

A_i	Interfacial area between fluid and solid domain [mm ²]
D_h	Hydraulic diameter [mm]
φ_{cf}	Heat flux through cell-interface [W m ⁻²]
\dot{q}_i	Total heat flux through the fluid-solid interface [W m ⁻²]
f	Friction factor
ΔP	Pressure drop [Pa]
U	Overall heat transfer coefficient [Wm ⁻² K ⁻¹]
H_f	Fin height [mm]
S_f	Fin pacing [mm]
L_f	Fin length [mm]
t_f	Fin thickness [mm]
T	Temperature [K]
C_p	Specific heat capacity [J kg ⁻¹ K ⁻¹]
Pr	Prandtl number
\dot{m}	Mass flow rate [g s ⁻¹]
Re	Reynolds number
u	Velocity [m s ⁻¹]
k	Thermal conductivity [W m ⁻¹ K ⁻¹]

Greek symbols

ϕ	Volume fraction of nanoparticles
μ	Dynamic viscosity [kg m ⁻¹ s ⁻¹]
ρ	Density [kg m ⁻³]

Sub and super scripts

p	Particulate
s	Solid
fl	Base fluid
eff	Effective
i	Inlet
b	Base
o	Outlet

Abbreviations

LMTD	Logarithmic mean temperature difference [K]
PEC	Performance evaluation criterion
sCO ₂	Supercritical carbon dioxide

References

- Baird, E.; Mohseni, K. Digitized Heat Transfer: A New Paradigm for Thermal Management of Compact Micro Systems. *IEEE Trans. Compon. Packag. Technol.* **2008**, *31*, 143–151. [\[CrossRef\]](#)
- Erbas, N.; Baysal, O. Micron-Level Actuators for Thermal Management of Microelectronic Devices. *Heat Transf. Eng.* **2009**, *30*, 138–147. [\[CrossRef\]](#)
- Saeed, M.; Berrouk, A.S.; Al Shehhi, M.S.; Al Wahedi, Y.F. Numerical investigation of the thermohydraulic characteristics of microchannel heat sinks using supercritical CO₂ as a coolant. *J. Supercrit. Fluids* **2021**, *176*, 105306. [\[CrossRef\]](#)
- Li, J.; Peterson, G.P. 3-Dimensional numerical optimization of silicon-based high performance parallel microchannel heat sink with liquid flow. *Int. J. Heat Mass Transf.* **2007**, *50*, 2895–2904. [\[CrossRef\]](#)
- Chai, L.; Xia, G.; Wang, L.; Zhou, M.; Cui, Z. Heat transfer enhancement in microchannel heat sinks with periodic expansion–contraction cross-sections. *Int. J. Heat Mass Transf.* **2013**, *62*, 741–751. [\[CrossRef\]](#)
- Zhang, F.; Wu, B.; Du, B. Heat transfer optimization based on finned microchannel heat sink. *Int. J. Therm. Sci.* **2022**, *172*, 107357. [\[CrossRef\]](#)
- Kumar, S.; Singh, P.K. A novel approach to manage temperature non-uniformity in minichannel heat sink by using intentional flow maldistribution. *Appl. Therm. Eng.* **2019**, *163*, 114403. [\[CrossRef\]](#)
- Khoshvaght-Aliabadi, M.; Sahamiyan, M.; Hesampour, M.; Sartipzadeh, O. Experimental study on cooling performance of sinusoidal-wavy minichannel heat sink. *Appl. Therm. Eng.* **2016**, *92*, 50–61. [\[CrossRef\]](#)
- Khoshvaght-Aliabadi, M.; Feizabadi, A.; Nouri, M. Design of novel geometries for minichannels to reduce junction temperature of heat sinks and enhance temperature uniformity. *Appl. Therm. Eng.* **2021**, *192*, 116926. [\[CrossRef\]](#)
- Chai, L.; Wang, L.; Bai, X. Thermohydraulic performance of microchannel heat sinks with triangular ribs on sidewalls–Part 2: Average fluid flow and heat transfer characteristics. *Int. J. Heat Mass Transf.* **2019**, *128*, 634–648. [\[CrossRef\]](#)
- Awais, A.A.; Saeed, M.; Kim, M.-H. Performance enhancement in minichannel heat sinks using supercritical carbon dioxide (sCO₂) as a coolant. *Int. J. Heat Mass Transf.* **2021**, *177*, 121539. [\[CrossRef\]](#)

12. Gong, L.; Kota, K.; Tao, W.; Joshi, Y. Parametric numerical study of flow and heat transfer in microchannels with wavy walls. *J. Heat Transf.* **2011**, *133*, 051702. [[CrossRef](#)]
13. Wang, Z.-H.; Wang, X.-D.; Yan, W.-M.; Duan, Y.-Y.; Lee, D.-J.; Xu, J.-L. Multi-parameters optimization for microchannel heat sink using inverse problem method. *Int. J. Heat Mass Transf.* **2011**, *54*, 2811–2819. [[CrossRef](#)]
14. Caney, N.; Marty, P.; Bigot, J. Friction losses and heat transfer of single-phase flow in a mini-channel. *Appl. Therm. Eng.* **2007**, *27*, 1715–1721. [[CrossRef](#)]
15. Tullius, J.; Tullius, T.K.; Bayazitoglu, Y. Optimization of short micro pin fins in minichannels. *Int. J. Heat Mass Transf.* **2012**, *55*, 3921–3932. [[CrossRef](#)]
16. Xie, X.; Liu, Z.; He, Y.; Tao, W. Numerical study of laminar heat transfer and pressure drop characteristics in a water-cooled minichannel heat sink. *Appl. Therm. Eng.* **2009**, *29*, 64–74. [[CrossRef](#)]
17. Naphon, P.; Wongwises, S. Investigation on the jet liquid impingement heat transfer for the central processing unit of personal computers. *Int. Commun. Heat Mass Transf.* **2010**, *37*, 822–826. [[CrossRef](#)]
18. Panão, M.; Guerreiro, J.; Moreira, A. Microprocessor cooling based on an intermittent multijet spray system. *Int. J. Heat Mass Transf.* **2012**, *55*, 2854–2863. [[CrossRef](#)]
19. Hu, H.; Ge, T.; Dai, Y.; Wang, R. Experimental study on water-cooled thermoelectric cooler for CPU under severe environment. *Int. J. Refrig.* **2016**, *62*, 30–38. [[CrossRef](#)]
20. Wang, X.-D.; Bin, A.; Xu, J.-L. Optimal geometric structure for nanofluid-cooled microchannel heat sink under various constraint conditions. *Energy Convers. Manag.* **2013**, *65*, 528–538. [[CrossRef](#)]
21. Peyghambarzadeh, S.; Hashemabadi, S.; Chabi, A.; Salimi, M. Performance of water based CuO and Al₂O₃ nanofluids in a Cu–Be alloy heat sink with rectangular microchannels. *Energy Convers. Manag.* **2014**, *86*, 28–38. [[CrossRef](#)]
22. Roberts, N.A.; Walker, D. Convective performance of nanofluids in commercial electronics cooling systems. *Appl. Therm. Eng.* **2010**, *30*, 2499–2504. [[CrossRef](#)]
23. Rafati, M.; Hamidi, A.; Niaser, M.S. Application of nanofluids in computer cooling systems (heat transfer performance of nanofluids). *Appl. Therm. Eng.* **2012**, *45*, 9–14. [[CrossRef](#)]
24. Jajja, S.A.; Ali, W.; Ali, H.M.; Ali, A.M. Water cooled minichannel heat sinks for microprocessor cooling: Effect of fin spacing. *Appl. Therm. Eng.* **2014**, *64*, 76–82. [[CrossRef](#)]
25. Ho, C.-J.; Chen, W.-C.; Yan, W.-M. Experimental study on cooling performance of minichannel heat sink using water-based MEPCM particles. *Int. Commun. Heat Mass Transf.* **2013**, *48*, 67–72. [[CrossRef](#)]
26. Naphon, P.; Nakharintr, L. Heat transfer of nanofluids in the mini-rectangular fin heat sinks. *Int. Commun. Heat Mass Transf.* **2013**, *40*, 25–31. [[CrossRef](#)]
27. Ijam, A.; Saidur, R.; Ganesan, P. Cooling of minichannel heat sink using nanofluids. *Int. Commun. Heat Mass Transf.* **2012**, *39*, 1188–1194. [[CrossRef](#)]
28. Rimbault, B.; Nguyen, C.; Galanis, N. Experimental investigation of CuO–water nanofluid flow and heat transfer inside a microchannel heat sink. *Int. J. Therm. Sci.* **2014**, *84*, 275–292. [[CrossRef](#)]
29. Keshavarz Moraveji, M.; Mohammadi Ardehali, R.; Ijam, A. CFD investigation of nanofluid effects (cooling performance and pressure drop) in mini-channel heat sink. *Int. Commun. Heat Mass Transf.* **2013**, *40*, 58–66. [[CrossRef](#)]
30. Afrand, M. Experimental study on thermal conductivity of ethylene glycol containing hybrid nano-additives and development of a new correlation. *Appl. Therm. Eng.* **2017**, *110*, 1111–1119. [[CrossRef](#)]
31. Dominic, A.; Devahdhanush, V.; Suresh, S. An experimental investigation on the effect of relative waviness on performance of minichannel heat sinks using water and nanofluids. *Heat Mass Transf.* **2022**, *58*, 247–262. [[CrossRef](#)]
32. Babar, H.; Wu, H.; Ali, H.M.; Shah, T.R.; Zhang, W. Staggered oriented airfoil shaped pin-fin heat sink: Investigating the efficacy of novel water based ferric oxide-silica hybrid nanofluid. *Int. J. Heat Mass Transf.* **2022**, *194*, 123085. [[CrossRef](#)]
33. Bazkhane, S.; Zahmatkesh, I. Taguchi-based sensitivity analysis of hydrodynamics and heat transfer of nanofluids in a microchannel heat sink (MCHS) having porous substrates. *Int. Commun. Heat Mass Transf.* **2020**, *118*, 104885. [[CrossRef](#)]
34. Nemati, H. A general equation based on entropy generation minimization to optimize plate fin heat sink. *Eng. J.* **2018**, *22*, 159–174. [[CrossRef](#)]
35. Chai, L.; Shaukat, R.; Wang, L.; Wang, H.S. A review on heat transfer and hydrodynamic characteristics of nano/microencapsulated phase change slurry (N/MPCS) in mini/microchannel heat sinks. *Appl. Therm. Eng.* **2018**, *135*, 334–349. [[CrossRef](#)]
36. Saeed, M.; Kim, M.-H. Heat transfer enhancement using nanofluids (Al₂O₃-H₂O) in mini-channel heatsinks. *Int. J. Heat Mass Transf.* **2018**, *120*, 671–682. [[CrossRef](#)]
37. Fronk, B.M.; Rattner, A.S. High-flux thermal management with supercritical fluids. *J. Heat Transf.* **2016**, *138*, 124501. [[CrossRef](#)]
38. Jung, S.Y.; Park, H. Experimental investigation of heat transfer of Al₂O₃ nanofluid in a microchannel heat sink. *Int. J. Heat Mass Transf.* **2021**, *179*, 121729. [[CrossRef](#)]
39. Bahiraei, M.; Monavari, A.; Naseri, M.; Moayedi, H. Irreversibility characteristics of a modified microchannel heat sink operated with nanofluid considering different shapes of nanoparticles. *Int. J. Heat Mass Transf.* **2020**, *151*, 119359. [[CrossRef](#)]
40. Yan, W.-M.; Ho, C.J.; Tseng, Y.-T.; Qin, C.; Rashidi, S. Numerical study on convective heat transfer of nanofluid in a minichannel heat sink with micro-encapsulated PCM-cooled ceiling. *Int. J. Heat Mass Transf.* **2020**, *153*, 119589. [[CrossRef](#)]
41. Ho, C.J.; Liao, J.-C.; Yan, W.-M.; Amani, M. Experimental study of transient thermal characteristics of nanofluid in a minichannel heat sink with MEPCM layer in its ceiling. *Int. J. Heat Mass Transf.* **2019**, *133*, 1041–1051. [[CrossRef](#)]

-
42. Chummar, A.; Harish, R. CFD simulation of laminar free convection flows of nanofluids in a cubical enclosure. *Mater. Today Proc.* **2022**, *51*, 1473–1481. [[CrossRef](#)]
 43. Ansys. Inc. *ANSYS, ANSYS CFX-Solver Theory Guide*; Ansys. Inc.: Canonsburg, PA, USA, 2011.
 44. Saeed, M.; Kim, M.-H. Numerical study on thermal hydraulic performance of water cooled mini-channel heat sinks. *Int. J. Refrig.* **2016**, *69*, 147–164. [[CrossRef](#)]